DOI: 10.13009/EUCASS2017-171

Numerical Simulation of a Rotating Detonation under Conditions of Premixed and Separate Injection of $H_2 - O_2$

Thomas Gaillard[⋆†], *Dmitry Davidenko*[⋆], *and Francis Dupoirieux*[⋆]
[⋆]*ONERA*
Chemin de la Hunière, BP 80100, 91123 PALAISEAU CEDEX, France
[†]Corresponding author

Abstract
This paper presents the numerical simulations of a Rotating Detonation (RD) propagating in a layer of combustible mixture, created by injection of gaseous hydrogen and oxygen. 3D Large Eddy Simulations (LES) of a reacting flow have been performed in a domain of planar geometry with different injector types operating in the regimes of premixed and separate propellant injection. A quasi-2D case with uniformly distributed premixed injection is first simulated to characterize the RD propagation under the most idealized conditions. Then, the simulations are performed with a 3D injector of the semi-impingement (SI) concept under the conditions of premixed and separate injection of the propellants at globally stoichiometric proportions. The case of separate propellant injection is the most realistic one. The computational results, represented by instantaneous and averaged flowfields, are analyzed to point out the changes in the conditions of RD propagation induced by the injection through discrete holes with respect to the distributed one and by the switching between the premixed and separate regimes. Besides the SI concept, an improved (Imp) concept for the injector has been designed to improve the mixing efficiency in the fresh mixture layer. Macroscopic quantities, such as the RD propagation speed, average parameters of the fresh mixture, and mixing efficiency are evaluated and compared in order to characterize the studied effects for the simulated cases.

1. Introduction

First studies of the operation of a Continuous Detonation Wave Rocket Engine (CDWRE) date back to the 1960s and were experimentally conducted both by Voitsekhovskii[1] and Nicholls and Cullen.[2] Since then, a group of LIH (Lavrentyev Institute of Hydrodynamics) researchers[3] has worked on the CDWRE by testing different combustion chamber geometries, injector designs and propellant mixtures, regarding the stabilization of the Rotating Detonation (RD). Theoretical interest in the thermodynamic cycle with detonation has been demonstrated by Zeldovich[4] and Wintenberger et al.,[5] and more recently by Davidenko et al.,[6] particularly devoted to rocket propulsion. Detonation propagation produces an additional pressure gain in the combustion chamber providing better performance than classical deflagration. That is why, it is generally considered that detonation engines have a great potential to succeed to the conventional engines with constant-pressure combustion.

With the increase of computing power, numerical simulation of RD has been strongly developed over the past decade. The first computation of a RD under 2D hypothesis by Zhdan[7] has paved the way towards the modeling of more realistic conditions of RD propagation regarding the experimental work. 3D simulations in an annular CDWRE chamber were carried out by Eude et al.[8] with premixed injection uniformly distributed over the injection wall. A comparative study of on RD propagation over injection slits of different shapes for premixed injection has been conducted by Liu et al.[9] They obtained RD instabilities produced by the dilution of the injected premix by the burnt gases. Schwer et al.[10] used periodic boundaries to propagate the RD over a 3D row of holes for premixed injection. They observed the pressure feedback from the chamber to the injector that prevented the mixture from being reinjected for a short time period after the detonation passage.

A first problem with injecting premixed propellants can happen during the blocking period: a deflagration can be initiated at the free interface between the fresh mixture and burnt gases and propagate upstream in the injector. A second problem, more dangerous, is the detonation transmission through the injection holes that can lead to severe engine deterioration. To preserve the safety of the experiments and avoid these two risks, the hole diameter has to be carefully chosen. For the deflagration, decreasing the diameter increases the thermal losses at walls, thus leading to

DOI: 10.13009/EUCASS2017-171

deflagration quenching. For the detonation transmission, a critical diameter can be defined as $d_{\text{crit}} = \lambda/\pi$, where λ is the detonation cell size. This threshold is about 20 μm for a stoichiometric mixture of gaseous H_2 and O_2 at a pressure of 1 MPa. For these two reasons, separate injection of the propellants is preferred.

Separate injection has negative consequences on the CDWRE performance. The main problem is to obtain fast and efficient mixing by turbulence while limiting the total pressure losses. As reported by Bykovskii et al.,[3] the experimental RD speed is often decreased by 20% compared to the theoretical Chapman-Jouguet speed. This difference may be due to heterogeneities of the fresh mixture and pressure losses. A lot of CDWRE experiments are conducted without a priori knowing the injector ability to create a sufficiently good mixture while mixing is thought to be essential for RD efficiency. That is why this numerical study is dedicated to the characterization and optimization of separate injection. Recent numerical works have been undertaken to propose new configurations for propellant mixing. Stoddard et al.[16,17] tried different geometries for separate injection of air and hydrogen with a single detonation propagation over a linear series of 10 injection elements. They wanted to study the expansion of burnt gases and the ability to refill the fresh mixture by propagating a real detonation. Driscoll et al.[18] characterized the mixing performance under non reacting flow conditions in a rotating detonation engine fed with H_2 and air. They compared several injection elements with different numbers of holes and with different arrangements to investigate the interactions providing optimum mixing. Such kind of simulation must be developed to find out more about unsteady process occurring during CDWRE operation.

In our previous studies, 3D Large Eddy Simulation (LES) were performed to simulate the mixing of H_2/O_2 propellant jets and to evaluate mixing efficiency and pressure losses in established[13] and transitory[19] injection regimes. We focused on understanding the mixing interactions at the scale of a single injection element. A particular injection element design called “semi-impinging” was selected based on the mixing efficiency and total pressure recovery criteria. The present paper deals with simulations of a RD propagation with two types of injector. A reference case uses uniformly distributed premixed injection. Second, the semi-impinging element is tested both in the premixed and separate injection regimes. Third, latest results with an improved injection element are presented for the separate injection regime. Finally, all the injector configurations are compared thanks to performance parameters such as RD speed and mixing efficiency.

2. Definition of the computational domain

2.1 RD propagation in classical annular geometry

The most often considered geometry for a CDWRE combustion chamber is annular, regarding both numerical and experimental studies. Its operation principle is schematically shown in Fig.1. The fuel and oxidizer (1) are fed through the injection wall (2) by holes. At the engine start, detonation initiation creates one or several RD fronts (3) that propagate in the layer of combustible mixture (4) formed by the propellant injection. The height of the RD front, h, and the spatial period, l, between successive fronts are proportional and depend on the propellants and injection conditions. When a stable operation regime is reached, RD propagate continuously in the same azimuthal direction thus having rotational motion about the chamber axis. Oblique shocks (5) are produced by RD in the burnt gases. Combustion products generated by RD expand in the chamber and discharge through the open end (6) of the duct.

2.2 Planar domain for RD propagation simulation

Although this paper is devoted to the analysis of RD propagation under realistic injection conditions, the simulations presented below consider a planar domain instead of an annular one. This choice is motivated by three reasons: (i) the geometry of the future CDWRE has not been decided yet; (ii) the objective of these computations is mainly to obtain the effect of the injection conditions on the RD propagation by avoiding coupling with other effects due to a particular chamber geometry; (iii) the computational cost of one simulation will be limited, allowing comparative computations with different conditions and during sufficiently long physical time to obtain established flowfields. Hence the effects due to the cylindrical wall curvature such as the detonation front reflection and radial gradients of flowfield parameters are not taken into account in the present study. Eude et al.[8] have shown that the 3D flowfield in an annular chamber is similar to a 2D flowfield if the radius of the annulus is large enough with respect to the duct width (radial distance between the cylindrical walls). For the same reasons as mentioned above, the viscous effects on the chamber walls are also neglected.

The 3D computational domain can be obtained by cutting and unrolling the annular geometry to obtain a planar one with periodicity conditions on the cutting surfaces. The RD fronts are assumed to be equidistant, meaning that the

DOI: 10.13009/EUCASS2017-171

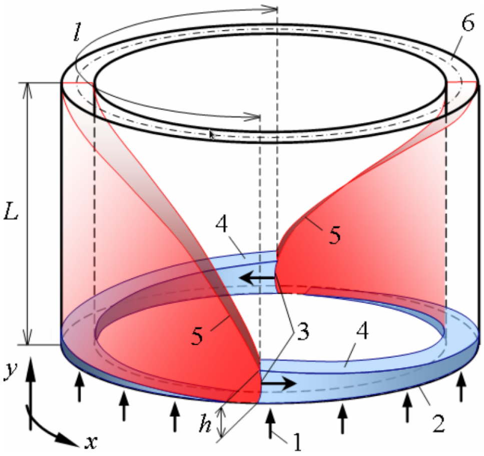

Figure 1: Principle of the CDWRE operation: 1 - propellant injection; 2 - injection wall; 3 - RD fronts; 4 - fresh mixture layer; 5 - oblique shocks; 6 - outlet section; h - height of RD front; l - spatial period between successive RD fronts; L - chamber length.

spatial period l and the RD velocity V_D are constant. Hence, the computational domain is chosen to cover only one period l as shown in Fig.2. The domain is composed of three parts:

- the injector of length L_j, represented either by a slot, as shown in Fig.2 or a series of injection holes as shown in Fig.3;
- the combustion chamber of length L, where the RD propagates;
- the divergent duct of length L_d, to ensure supersonic outflow conditions and make the simulated flow independent of the downstream conditions.

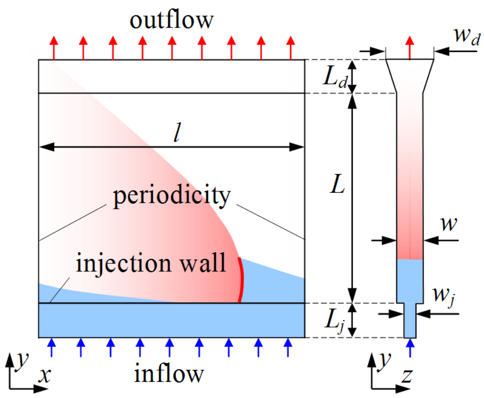

Figure 2: Schematic of the computational domain for RD simulation.

In this paper, the spatial period is l = 50 mm. It is a lower estimation from the relations proposed by Bykovskii et al.[3] if one considers a 1 mm detonation cell size. The chamber length is L = 20 mm. This value is large enough to prevent the RD propagation from being affected by the duct divergence. It is confirmed both experimentally[3] and numerically[14] that $L = 2h$ is sufficient.

The propellants are both injected with a total temperature of 300 K. Their mass flow rates are globally at stoichiometric proportions with a total mass flow rate per unit area of the chamber cross section is 100 kg/(s·m^2). Such conditions can correspond to ground testing of a model CDWRE.

DOI: 10.13009/EUCASS2017-171

2.3 3D injector of semi-impinging configuration

The considered injection configuration has been selected among various designs in a previous study by the authors.[13] It is a periodic pattern, in both coordinate directions on the injection wall, of unlike semi-impinging jets, which provides better mixing efficiency than purely impinging or sheared configurations, on the one hand, and than patterns with symmetric pairs of injection elements, on the other hand. Two neighboring injection elements are shown in Fig.3. Their arrangement in a row along the x-axis features their layout on the injector face (2) in Fig.1. The angle of impact α between the two jets is 60° and the angle of the feeding pipes with the direction normal to the injector face is 30°.

The elliptical sections of the injection holes have parallel major axes. The angle β between the line passing through the centers of the ellipses and their major axes is equal to 45°. In order to avoid intersection of the feeding pipes from neighboring injection elements, each pair of pipes is set at the angle γ equal to 13° with respect to the x-axis as shown in Fig.3.

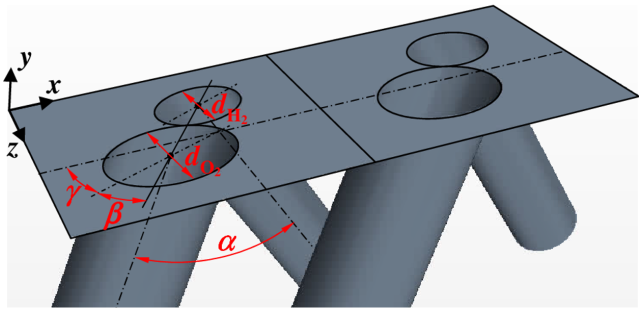

Figure 3: 3D view of two injection elements in a row.

In the 3D simulations presented below, 21 injection elements are set in a single row along the x-axis by the same way as illustrated in Fig.3. The total area of round injection holes represents 20% of the injector face area, as for the injector domain in Fig.2. The diameters of H_2 and O_2 holes are $d_{H_2} = 0.71$ mm and $d_{O_2} = 1$ mm respectively. The element dimensions along the x and z-axis are 2.45 mm and 2.4 mm respectively.

3. Numerical strategy with the CEDRE code

The computational results presented in this paper were obtained using the CEDRE code. It is a CFD platform developed at ONERA[11,12] for numerical simulations applied to energetics and propulsion. CEDRE is composed of multiple solvers based on a finite-volume method for general unstructured meshes. For the present study, Navier-Stokes equations were solved to simulate a reactive flow of multispecies compressible gas. Flow turbulence is simulated using the LES approach with the Smagorinsky subgrid viscosity model. Convective fluxes are determined using the classical HLLC scheme for Riemann problem solution. Second-order accuracy in space is reached due to a MUSCL scheme with the Van Leer slope limiter for the convective fluxes and the central-difference scheme for the viscous fluxes. Time integration is realized using an accurate implicit scheme with the GMRES method for solving the linearized equation system.

The reactive mixture contains 6 chemical species (H_2, O_2, H_2O, H, O, OH) treated as ideal gases with classical temperature-dependent properties. The chemical kinetic model is defined by 7 reversible reactions. This model was tested by Davidenko et al.[14] and considered accurate enough for detonation simulation compared to more complex mechanisms. Constant Prandtl and Schmidt numbers are adopted to define molecular transport properties of the species. As the present study is focused on the mixing process between the fresh propellants, the transport coefficients of H_2 and O_2 were determined for their mixture at stoichiometric proportions. For the other species, pure species properties are used.

For the RD simulations in the domain presented in Fig.2, the chemical kinetic model was active in the combustion chamber and divergent duct, whereas in the injector, the gas mixture was treated as non-reactive. This was required in the case of premixed injection in order to prevent detonation propagation inside the injector. It should be stressed that the premixed injection is considered here with the only purpose to identify the flowfield changes between the premixed and separate injection modes and not as a real operation mode.

Before performing RD simulations, the CEDRE code was tested on 1D cases. First, a CJ detonation was simulated. The inner structure of the detonation is not resolved to limit the computational cost and also because only stable propagation regimes are of interest in this paper. Hence, the mesh size can be adapted to at least compute well the theoretical detonation velocity (2836 m/s at 0.1 MPa and 300 K) and the CJ state of the burnt gases. It was observed that a

DOI: 10.13009/EUCASS2017-171

100 μm mesh size is sufficient for this two purposes. Moreover, most of known RDE simulations were performed with relatively coarse resolution but sufficient for correct prediction of the detonation speed and overall change of flow parameters. Second, freely propagating laminar flames were simulated to study the capability of treating the deflagration front at the contact surface between the fresh mixture and burnt gases. No particular combustion model is used to treat this front. This simple simulation gives a first-order prediction for the deflagration speed. The flames were initiated in a range of pressure corresponding to the pressure evolution along the deflagration front due to the expansion process behind the RD. It was observed that at the beginning of the expansion (resp. the end of the expansion), the deflagration speed is overestimated (resp. underestimated) with respect to the reference simulation with the PREMIX code from CHEMKIN-II. However, the error in the laminar flame speed will not be very important in the RD simulations because the rate of fresh mixture consumption by the deflagration is typically an order of magnitude smaller than that by the detonation.

4. Simulated cases of RD propagation

The following results are presented in different frameworks. First, the most ideal propagation is obtained in a quasi-2D configuration shown in Fig.2. Then, 3D simulations of RD propagation are conducted with the semi-impinging injector design (named SI) introduced in Fig.3. The simulated flowfields are compared for the premixed and separate injection regimes. Finally, the last case shows the RD propagation using an improved injection element (named Imp) able to increase the mixture quality in the separate injection regime.

4.1 Case 2D: ideal propagation case

The ideal propagation of the RD is obtained in a quasi-2D configuration with the injection of a stoichiometric $H_2 - O_2$ mixture uniformly distributed along the injection slot. The geometrical configuration shown in Fig.2 is set with the following parameters: $L_j = L_d = 2$ mm, $w_j/w = 0.2$ and $w_d/w = 3$. The computational mesh used for this case is structured in the zone of RD propagation with square cells of 100 μm size. It has only one layer of cells in the z direction (so-called quasi-2D case) meaning that the flow is considered uniform in this direction. It is a reference case that will be compared with the 3D results presented later. The instantaneous fields of pressure, temperature, H_2O and H mass fractions (Y_{H_2O} and Y_H fields respectively) are presented in Fig.4.

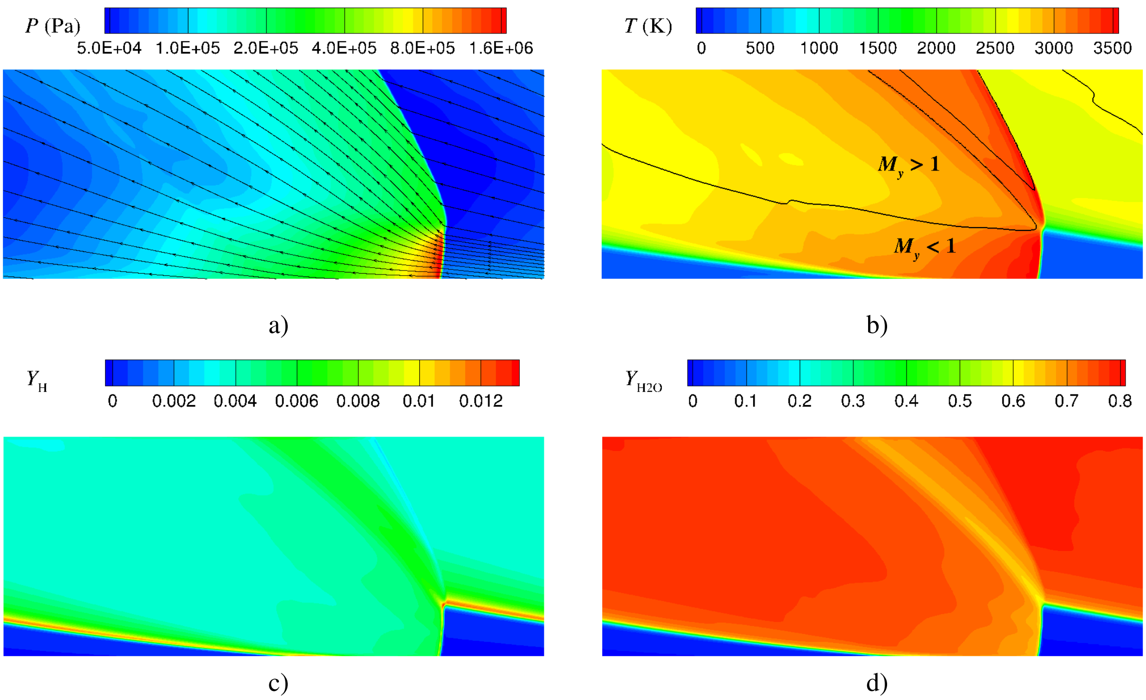

Figure 4: Instantaneous flowfields from the quasi-2D simulation: a) static pressure with streamlines in the moving reference frame attached to the RD front; b) static temperature with the $M_y = 1$ contour; c) H-radical mass fraction; d) H_2O mass fraction.

DOI: 10.13009/EUCASS2017-171

In the pressure field, a high-pressure zone is produced in the burnt gases behind the RD front. The oblique shock is also indicated by the pressure increase in the burnt gases. Streamline contours are plotted in the moving reference frame attached to the RD. In the temperature field, one can recognize the main elements of the flow structure shown in Fig.1. The sonic contour of Mach number M_y defined from the y-wise component of the flow velocity is also traced in this field. One can observe from these two figures the expansion process of the hot gases behind the RD, which is indicated by the diverging streamlines and decreasing pressure and temperature. This expansion permits reinjecting the fresh mixture at a distance from the RD of approximately 25% of the l period according to the presented fields. The acceleration of the expanding hot gazes results in a supersonic flow on the major part of the cross section at $y = L$, where the $M_y = 1$ contour is below this section. The H_2O mass fraction field is closely related to the temperature field because the high fraction of this species points out the completeness of the combustion process and the corresponding temperature rise. The RD burns out all the stoichiometric mixture passing through its front. In the combustion products, the decrease of Y_{H_2O} behind the oblique shockwave is explained by the dissociation effects linked to the temperature increase by the shock. Finally, the field of H-radical fraction helps to identify the reaction fronts where H radicals are produced during the ignition. The highest level of H radical is found above the fresh mixture layer, meaning that a deflagration appears at the interface between the fresh and burnt gases. This deflagration is transformed in a wake behind the oblique shockwave, which disrupts the $M_y = 1$ contour. H radical is less present in the RD front because it is much thinner than the deflagration front, so the H-radical peak is less marked with the available spatial resolution.

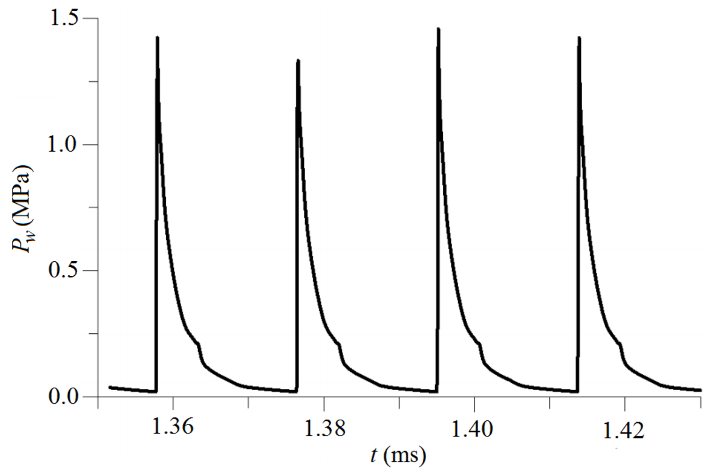

Figure 5: Time history of the wall pressure P_w on the injection wall for the quasi-2D configuration.

It takes between 6 and 9 rotation periods to reach a stable propagation regime. The pressure signal $P_w(t)$ is recorded by a numerical sensor located on the injection wall and plotted in Fig.5. The regularity of pressure peaks appearances demonstrates the stable RD propagation. One can estimate that a rotation period lasts about 18.7 µs. Consequently, the RD propagation speed is about 2679 m/s. Taking into account the x-wise component of the mean velocity in the fresh mixture layer, the RD speed with respect to the fresh mixture flow is about 2714 m/s, which is 4% lower than the CJ detonation speed determined for the mean pressure and temperature in the fresh mixture in front of the RD. The fresh mixture parameters obtained along a vertical line in front of the RD are reported in Tab.1.

4.2 Numerical techniques for 3D configurations treatment

4.2.1 Meshing, initial and boundary conditions

The 3D domain is meshed with cubic cells of 100 µm size in the lower part of the chamber subdomain ($y \leq 12.8$ mm). In the upper part ($y \geq 12.8$ mm), the mesh is progressively coarsened up to 400 µm. Refined results with 50 µm cells were also obtained but are not presented in this paper because the overall flowfields remained quite unchanged, as well as the RD velocity and other macroscopic parameters. The initial and boundary conditions used to simulate the RD with the injector SI are displayed in Fig.6.

The initial conditions correspond to the final state of the quasi-2D results obtained after stabilization of the RD propagation. It is important to note in Fig.6 that the RD propagation is initially oriented toward the direction of O_2 injection (let us remind that the O_2 feeding tubes are of larger diameter). Constant mass flux, total temperature and gaz composition are imposed at the inlet boundaries (1). Inviscid flow conditions are used on boundaries representing the

DOI: 10.13009/EUCASS2017-171

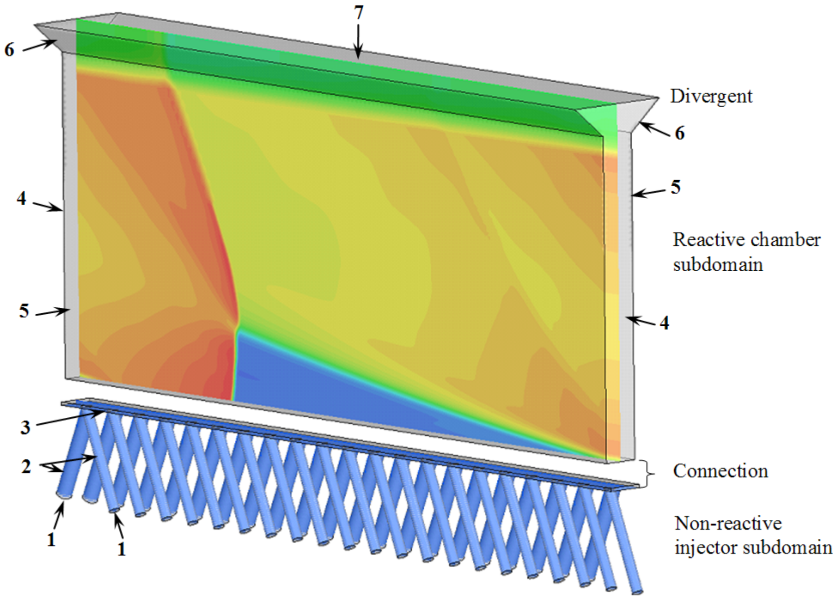

Figure 6: Computational domain split into the injector and chamber subdomains with schematic representation of the initial conditions. Boundary types: 1 - propellant inlet; 2 - walls of the feeding pipes; 3 - injector face wall; 4 - periodic boundaries; 5 - chamber walls; 6 - divergent duct walls; 7 - outlet.

walls of the injector feeding tubes (2), the injector face wall (3) as well as the divergent duct (6). Periodicity conditions are applied on the opposite boundaries of the chamber subdomain (4) and (5). Finally, supersonic outflow conditions are applied on the exit (7).

4.2.2 Averaging procedures for 3D data post-processing

No perturbations are observed in the quasi-2D fields because of the perfect continuity of the fresh mixture layer and the supersonic outflow created by the divergent duct. In contrast, the fresh mixture layer created by the injector with discrete holes in the 3D configurations is intermittent due to the presence of burnt gases and its structure can be very different along the z-direction. Moreover, when the RD consumes such a layer, it produces shocks and acoustic waves in the flowfield. In order to compare the 3D and quasi-2D results, an averaging procedure is required to eliminate the spatial heterogeneities and temporal fluctuations while keeping the overall flow structure for the analysis. Therefore, space and time averaged fields are needed for the 3D configurations. The averaging procedure is defined similarly to what Schwer et al. proposed in their study.[10] For N snapshots extracted every 1 µs, the solution is translated to set the N RD fronts at the same x_{front} coordinate, respecting the periodicity conditions. The N translated snapshots are first space averaged on the K cells along the z-direction and then time averaged according to the mass-weighted formulation:

$$< \widetilde{q}_{i,j} >= \frac{\sum_{n}^{N}\sum_{k}^{K}(\rho q)^{n}_{i,j,k}}{\sum_{n}^{N}\sum_{k}^{K}\rho^{n}_{i,j,k}} \tag{1}$$

where $< \widetilde{q}_{i,j} >$ represent 2D fields of the mass-averaged quantities. i, j and k are the indices along the x, y and z directions respectively. ρ is the density. K is the number of cells along the z direction. Formula (1) is applied for all variables except for density and pressure where a simple arithmetic average is performed.

A second procedure is related to the characterization of the fresh mixture layer in front of the RD. In 3D, a control volume is determined by the following coordinate extents. The x-range is defined from the RD front position $x_{\min} = x_{\mathrm{front}}$ to $x_{\max} = x_{\min} + l/N_{\mathrm{inj}}$, where $N_{\mathrm{inj}} = 21$ is the number of injection elements along the x direction. The y-range is defined from the injector face $y_{\min} = 0$ to $y_{\max}$ to be specified for each particular treatment. The z-range from $z_{\min} = 0$ to $z_{\max} = w$ covers the width of the chamber duct. Flow parameters are averaged within the sliding control volume for each snapshot by analogy with the spatial and temporal average described above.

DOI: 10.13009/EUCASS2017-171

4.3 3D propagation regimes with the SI injector

4.3.1 Case SIP: premixed injection regime

The first case of the RD propagation with the SI injector presented here corresponds to the injection of fully premixed propellants and named SIP. Although such a regime is not realistic yet in experimental operation of a CDWRE, it is first simulated because it is interesting to examine the difference with the fully separate injection. Figure 7 presents instantaneous fields at the median z-coordinate. This figure illustrates the unsteady and 3D character of the flow, especially in the fresh mixture layer. The snapshots of temperature and H-radical mass fraction show propellant jets surrounded with combustion products. Due to the non-uniformity of the fresh mixture layer, the RD front is not smooth resulting in a perturbed flow behind it. As the RD periodically crosses a regular pattern of propellant jets, it leads to the formation of acoustic waves with equidistant circular fronts behind the RD.[15] The acoustic perturbations generated by the previous RD interact with the present one thus increasing the overall level of fluctuations. One can also see from the H-radical snapshot that deflagration fronts are formed around the premixed propellant jets immediately from the injection plane so that the flame surface becomes very developed.

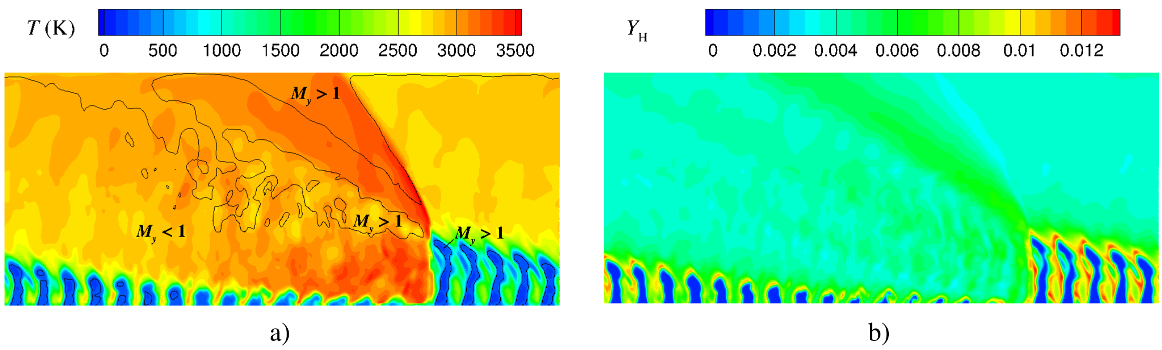

Figure 7: Instantaneous flowfields for Case SIP: a) static temperature with the M_y = 1 contour; b) H-radical mass fraction.

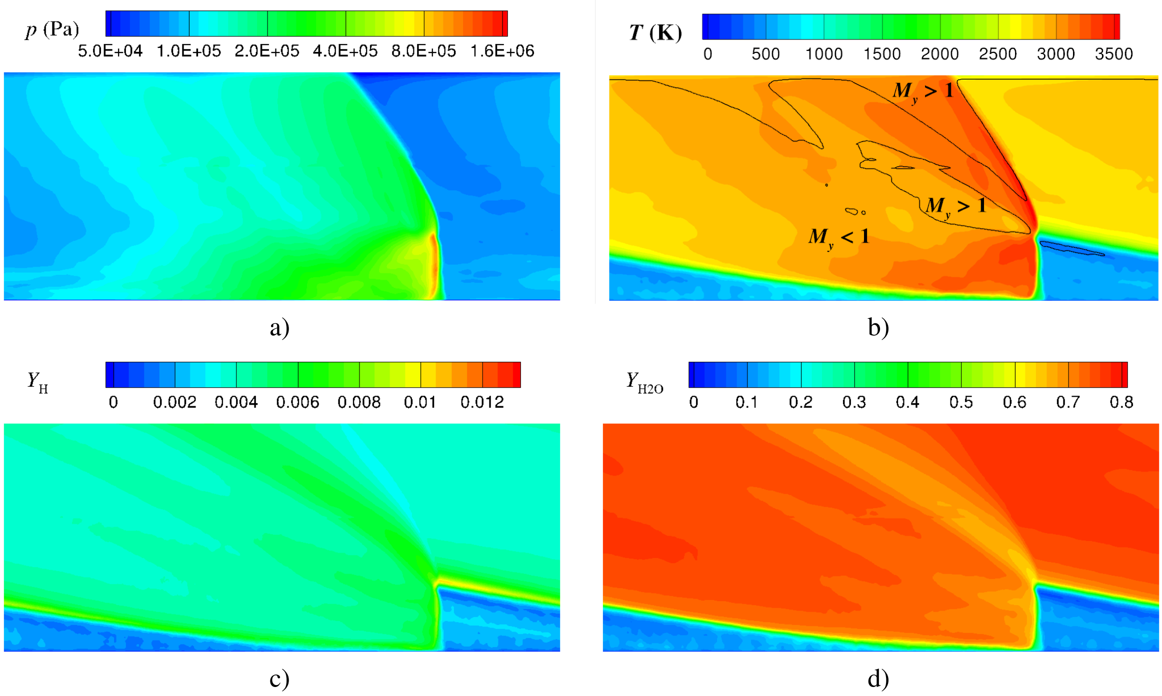

Figure 8: Averaged flowfields for Case SIP: a) static pressure; b) static temperature with the M_y = 1 contour; c) H-radical mass fraction; d) H_2O mass fraction.

After the flowfield establishment, 60 snapshots are extracted every 1 μs and averaged to obtain the results pre-

DOI: 10.13009/EUCASS2017-171

sented in Fig.8 which can be compared with Case 2D (see Fig.2) using distributed injection. The overall flow structure remain very similar for the two cases. Nevertheless, the pressure and temperature increase in the RD front of Case SIP is significantly reduced. The layer of fresh mixture is hotter on average (around 500 K) because of the dilution with burnt gases as shown in the Y_{H_2O} field. The production of Y_{H_2O} by the RD remains high and similar to Case 2D because of the premixed state of the injected propellants.

The expansion process behind the RD front has lower intensity in Case SIP. As a result, the burnt gases behind the RD are less accelerated as it is indicated by the reduced area above the $M_y = 1$ contour in Fig.7a and 8b. Consequently, expanded gases in front of the oblique shock have higher pressure and temperature than in Case 2D.

At the top of the average layer of fresh mixture, a deflagration front can be seen in the H-radical mass fraction field as in Case 2D. Moreover, the presence of H in the mixture layer accounts for the developed deflagrations around the premixed jets already seen in Fig.7b.

All these negative effects are due to the presence of combustion products, either remaining from the previous RD or generated by deflagration, in the fresh mixture layer of Case SIP, which becomes less dense in terms of mass and chemical energy.

4.3.2 Case SIS: separate injection regime

Case SIS represents established RD propagation with fully separate propellant injection, which represents the most realistic case. The instantaneous temperature and H-mass fraction fields are presented in Fig.9 and show that the perturbations are strongly intensified in comparison with Case SIP. Especially, the RD front is less visible because it is more subjected to the chaotic behavior of the fresh mixture layer. Pockets of unburnt gases can be seen behind the RD in the temperature field, meaning that mixing between the propellants is incomplete in the fresh mixture layer. These pockets disappear farther because the remaining propellants are finally mixed and consumed. The averaged results obtained with the same number of snapshots and sampling period as in Case SIP are presented in Fig.10.

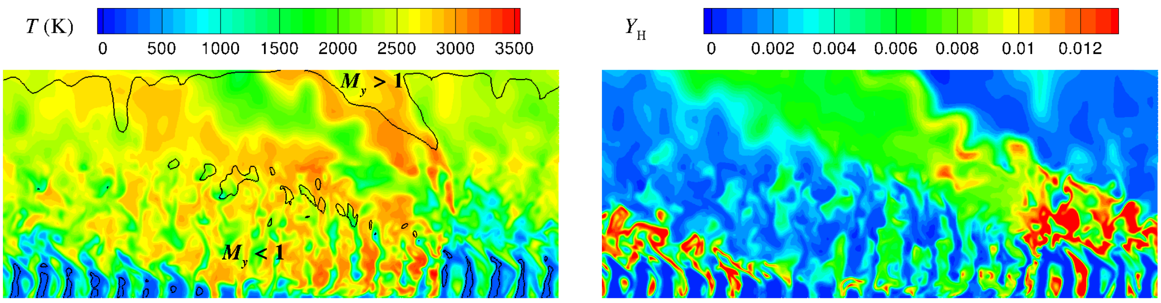

a) b)

Figure 9: Instantaneous flowfields for Case SIS: a) static temperature with the $M_y = 1$ contour; b) H-radical mass fraction.

In the temperature field, the $M_y = 1$ contour indicates further reduction of the area of supersonic flow in the y direction compared to Fig.8b of Case SIP and Fig.4b of Case 2D. Hence, the flow of combustion products is less accelerated during the expansion process behind the RD meaning that the RD is less efficient with the separate injection. In the pressure field, the RD front is strongly attenuated because it is highly perturbed both in space and time. Moreover, the flow compression is not uniform along the RD front. The zone of relatively high pressure faces the upper half of the cold fresh mixture layer where the propellant mixing is better than in the lower half. The overall pressure increase in the detonation wave is significantly reduced with respect to Case SIP because of incomplete mixing of separately injected propellants. An additional notable difference consists in intense combustion in a layer above the cold layer of fresh mixture, which is indicated by high levels of H-radical and H_2O fractions before and after the RD and oblique shock.

The field of H_2O fraction in Fig.10d displays a stratified distribution of this species with distinct layers in the burnt gas zone and great overall variation in the vertical direction, which is very contrasted with the corresponding fields of Cases 2D and SIP.

By analyzing the gas composition throughout the flowfield, specific zones can be identified as delimited by black contour lines in the averaged H_2O mass fraction field. In the fresh mixture layer, three zones are listed: the lower zone (1) is mainly filled with O_2 and less with H_2 and burnt gases; the intermediate zone (2) contains propellants in stoichiometric proportions but partially unmixed and diluted with burnt gases; the upper zone (3) is fuel-rich and strongly diluted with burnt gases. Three corresponding zones are delimited in the combustion products behind the RD:

DOI: 10.13009/EUCASS2017-171

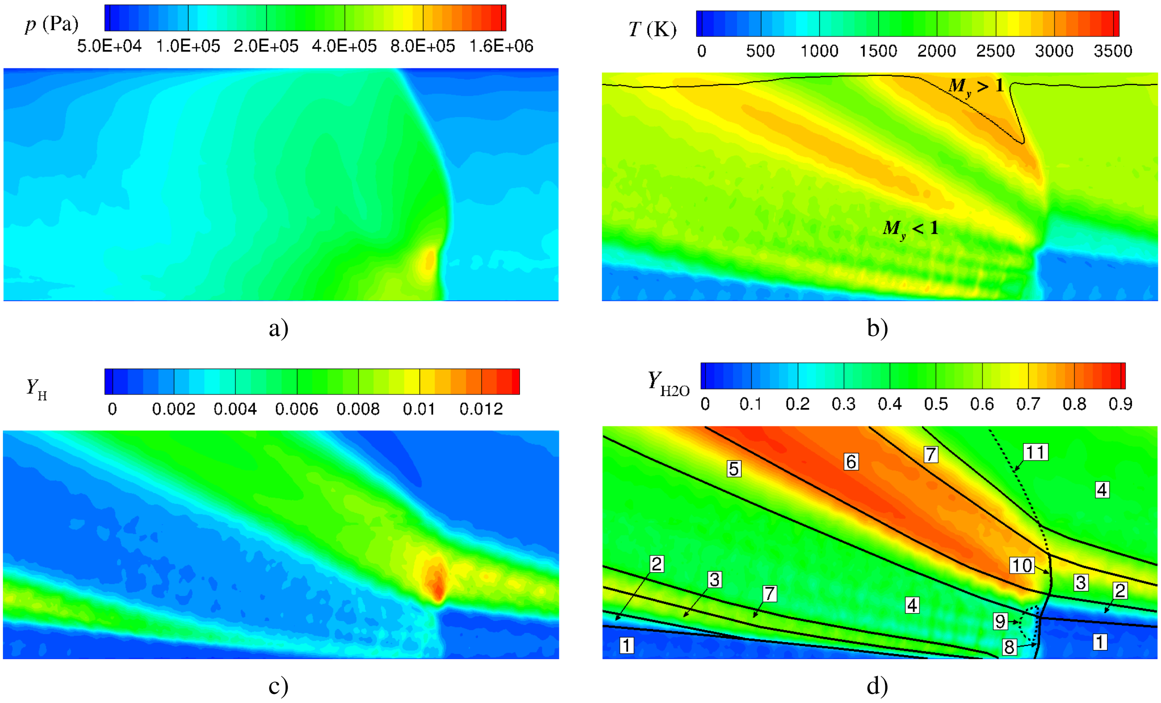

Figure 10: Averaged flowfields for Case SIS: a) static pressure; b) static temperature with the M_y = 1 contour; c) H-radical mass fraction; d) H_2O mass fraction. Black contours define the following zones: 1 - oxidizer-rich fresh mixture; 2 - nearly stoichiometric fresh mixture; 3 - fuel-rich fresh mixture diluted with burnt gases; 4 - oxidiser-rich combustion products from RD; 5 - nearly stoichiometric combustion products from RD; 6 - fuel-rich combustion products from RD; 7 - nearly stoichiometric combustion products from diffusion flame; 8 - RD front; 9 - high-pressure zone behind the RD front; 10 - degenerating RD front; 11 - oblique shock.

the oxidizer-rich zone (4) with a relatively low level of H_2O mass fraction; the nearly stoichiometric zone (5), across which the H_2O mass fraction rapidly increases; and the fuel-rich zone (6) with the highest level of H_2O mass fraction. The last zone (7) represents a nearly stoichiometric layer between the fuel-rich zone (3) and oxidizer-rich zone (4) resulting from the previous RD. This particular zone (7) produces H_2O similarly to a turbulent diffusion flame.

The RD propagation is driven by the most intense part of its front, which consumes mixed propellants from zones (1) and (2) and creates a zone of elevated pressure (9). The poor mixing in zone (1) near the injector face results in a less intense RD as well as in zone (3) with the lack of oxidizer and strong dilution with burnt gases. The upper part of the RD front (10) progressively degenerates and transforms into an oblique shock (11).

4.4 Case Imp: improved mixing in the separate regime

From the previous section, it can be stated that injector SI is not really efficient in mixing of separately fed propellants. Quantitative results on the injector performance will be delivered in section 5. For now, a new injector design called Imp is proposed in order to create a more homogeneous fresh mixture layer with the separate injection regime. The Imp design is not presented for confidentiality reasons and only the simulated flowfield will be discussed in comparison with Case SIS.

Average temperature and H_2O mass fraction fields are shown in Fig.11 and can be compared to the same variables of Case SIS in Fig.10b and d. The RD front is better marked in Case Imp than in Case SIS. The benefit of injector Imp is demonstrated by the temperature and H_2O fraction globally increased proving that the propellant mixture is more homogeneous and combustion is more efficient.

DOI: 10.13009/EUCASS2017-171

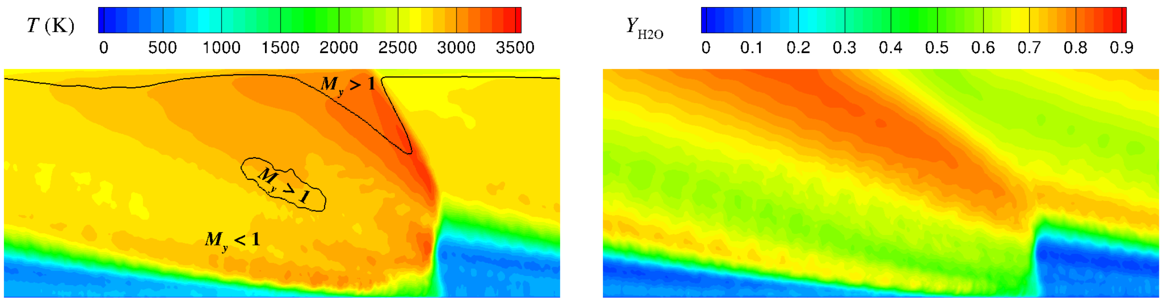

a) b)

Figure 11: Averaged flowfields for Case Imp: a) static temperature with the $M_y = 1$ contour; b) H_2O mass fraction.

5. Characterization of the injector performance

5.1 Average mixture parameters and RD propagation speed

To compare the performance of the 2D, SI and Imp injectors, macroscopic parameters are first determined, namely the average mixture properties in the control volume (pressure p_m, temperature T_m and longitudinal flow velocity $V_{x,m}$) and the RD propagation speed V_D. The mixture properties are obtained with equation (1) or arithmetic average for pressure. The height $y_{\max}$ of the control volume (or the vertical line in Case 2D) is defined as follows:

- For premixed Cases 2D and SIP, $y_{\max}$ is determined by the position of the deflagration front on the upper boundary of the fresh mixture layer. The premixed state of the propellant makes it easy to locate the deflagration by searching for the maximum of the H-radical which is then the $y_{\max}$ position.
- For separate Cases SIS and Imp, the height $y_{\max}$ is more difficult to obtain because the deflagration front is not clearly visible. Instead, a mass conservation argument is applied, meaning that the whole mass in the control volume has to correspond to the mass injected during one refill period by one injection element.

The RD speed can be obtained by tracking the displacement of the RD front between two consecutive snapshots extracted with a 1 µs sampling period. Considering the N snapshots, a global arithmetic average is then produced with the $N - 1$ local values of the RD speed. It is also estimated the theoretical CJ speed D_{CJ} based on the average mixture parameters in the control volume and the difference with respect to the fresh mixture flow $D = V_D - V_{x,m}$. All of these parameters are given in Tab.1.

Case	$y_{\max}$ **(mm)**	p_m **(kPa)**	T_m **(K)**	$V_{x,m}$ **(m/s)**	V_D **(m/s)**	D_{CJ} **(m/s)**	$(D - D_{\mathrm{CJ}})/D_{\mathrm{CJ}}$
2D	4.9	62.8	238	-35	2679	2825	-3.9%
SIP	6.6	83.7	563.4	22.7	2828	2681	4.6%
SIS	8.1	138.6	633.3	114.2	2166	2549	-19.5%
Imp	11.3	94.9	816.8	-76	2600	2599	3.0%

Table 1: Average fresh mixture parameters in the control volume and RD propagation speed for the simulated cases.

Case 2D represents the reference ideal case of RD propagation in fully premixed propellants without dilution. T_m is low because the layer of fresh mixture only contains fresh gases and the flow has an important vertical velocity. D is close to D_{CJ} meaning that the CJ theory can predict the RD propagation speed with an error less than 4%. In comparison with the average conditions in the fresh mixture layer of Case 2D, the pressure is higher by a factor of 1.33 (weaker flow expansion after RD) and the static temperature is higher by 325 K (presence of combustion products) in Case SIP. The value $y_{\max}$ is greater because the layer of fresh mixture is thickened by the hot-gas effects. One can also note that the x-component of velocity has different signs. It is negative in Case 2D mainly because of a positive x-wise pressure gradient in the fresh mixture layer. In spite of the same factor also present in Case SIP, the velocity sign is due to the orientation of the larger feeding tubes, which create an overall positive momentum of fresh mixture in the x direction. An interesting fact is that, in spite of the heterogeneity of the fresh mixture layer, D differs only by 4.6% from D_{CJ} determined for the average conditions in the control volume.

DOI: 10.13009/EUCASS2017-171

For the two separate Cases, y_{max} is greater than for the premixed ones due to the y_{max} definition. It can be noted that the more is y_{max}, the more is T_m because the control volume contains more burnt gases. The advantage of injector Imp over injector SI is proved by comparing V_D. Case SIS experiences large-scale mixture heterogeneities while they are strongly reduced in Case Imp. The efficient mixing process obtained with injector Imp helps the RD propagate at elevated speed. In particular, the CJ theory can no longer be applied to Case SIS to predict the RD speed. However, it still gives a good prediction for Case Imp.

5.2 Evaluation of the injector efficiency

To compare the injector efficiency for the studied cases, three parameters of interest are defined and given in Tab.2: the efficiency of combustion by the RD, η_D, the burnt gas fraction in the control volume $m_{BG}/m_{inj,elt}$ and the global mixing efficiency η_{mix}.

Case	η_D	$m_{BG}/m_{inj,elt}$	η_{mix}
2D	0.9	0.01	1
SIP	0,72	0,15	1
SIS	0,182	0,148	[0,182 ; 0,33]
Imp	0,482	0,223	[0,482 ; 0,705]

Table 2: Performance characteristics of the studied injectors.

$\eta_D = m_{st}/m_{inj,elt}$ represents the mass of propellants mixed at stoichiometric proportions that the RD can burnt with respect to the total mass injected by one element during a refill period. For Cases 2D and SIP, m_{st} is simply the integration of the quantity $\rho(Y_{H_2} + Y_{O_2})$ in the control volume because the fresh mixture is always in premixed state. $m_{inj,elt}$ is obtained given the total mass of injected propellants during the time period $\tau_D = l/(N_{inj}V_D)$. For Cases SIS and Imp, m_{st} is evaluated with a distinction between the mixture at stoichiometric proportions and excess of H_2 or O_2. m_{BG} represents the remaining mass of all gases (Burnt Gases) in the control volume excepting H_2 and O_2. Finally, η_{mix} quantifies the global potential for an injector to create a stoichiometric mixture. It is always 1 when propellants are initially in premixed state. For Cases SIS and Imp, η_{mix} cannot be estimated precisely because a part of the stoichiometric mixture that is formed during a refill period may be lost by deflagration. It means that m_{BG} contains both the combustion products from the previous RD and the actual losses by deflagration, which are difficult to distinguish. Two hypothesis can be made to give an interval for η_{mix}: (i) the lower estimation is obtained assuming that all the burnt gases come from the previous RD ($\eta_{mix} = m_{st}/m_{inj,elt}$), (ii) the upper estimation is obtained assuming that all the burnt gases are produced by deflagration losses ($\eta_{mix} = (m_{st} + m_{BG})/m_{inj,elt}$).

For Case 2D, η_D indicates that 90% of the injected mixture can be consumed by the RD meaning that 10% is lost by deflagration. For Case SIP, the loss of propellant mass increases to 28% owing to much more developed surface of flame front around the premixed propellant jets. With the uniform injection of Case 2D, practically no burnt gases $(m_{BG})/m_{inj,elt} = 0.01$) are found in the layer of fresh mixture. For Case SIP, 15% of the average mixture in the control volume are burnt gases whereas at least 13% of the mass burnt by deflagration is situated above the y_{max} limit of the control volume.

For Case SIS, the estimation of η_D shows that not more than 18% of the injected propellant mass is mixed and can be burnt by the detonation (the remaining part is however mixed and burnt behind the RD); nearly 70% of this mass remain unmixed due to the short time period between successive RD and the effect of propellant separate injection; almost 15% of remaining mass is represented by burnt gases, which can be either residual from the previous RD or generated by combustion of mixed fresh propellants. Case Imp produces much more mixture in stoichiometric proportions with an increase in η_D to almost 50% whereas η_{mix} is more than doubled compared to Case SIS.

6. Conclusion

A numerical study has been carried out providing an important set of simulation results on the stable propagation of a RD fed with the H_2 and O_2 gaseous propellants. Different injection regimes have been analyzed with increasing complexity of the propellant injection and mixing processes from an idealistic one with premixed uniformly distributed injection to the most realistic ones with separate injection through discrete holes (SI and Imp concepts). The simulation results for the different injection regimes have been systematically compared in order to provide physical interpretation of the observed changes related to the RD propagation conditions and efficiency of the combustion process. The 3D simulation results have been analyzed by considering instantaneous and averaged flowfields. Dedicated methods have

DOI: 10.13009/EUCASS2017-171

been developed to evaluate the RD propagation speed, average conditions in the fresh mixture layer and efficiency of the mixing and combustion processes.

By simulating the established RD propagation over a series of injection elements with periodic conditions on the lateral boundaries, it was possible to study the dynamic behavior of the injector as well as the formation of the fresh mixture layer between two consecutive passages of the RD. Several important findings have been made by analyzing the simulation results.

The use of discrete holes for propellant injection induces conditions for fresh mixture dilution with hot gases, which can either remain from the previous RD passage or be produced by combustion of the injected propellants. In the case of premixed injection through discrete holes, nearly 30% of the injected mass is consumed by deflagrative combustion because of a developed flame surface around the propellant jets. The dilution with hot gases results in considerable reduction of the pressure rise across the detonation wave and overall pressure decrease on the injection wall but not necessarily in a decrease of the RD propagation speed, which remains high due to the hot fresh mixture. In spite of the heterogeneities within the fresh mixture layer, the RD propagation speed differs by only a few percent from the CJ detonation speed determined for the fresh mixture average conditions in front of the RD.

With the separate propellant injection by injector SI, the main negative factor is the creation of large-scales heterogeneities. This separation of the propellants results in poor mixing efficiency (between 18% and 33%) within the fresh mixture layer and, as a consequence, in only 18% of fresh propellants burnt by detonation as well as globally incomplete combustion. The identification and explication of the propellant separation effect is a very important finding of this study, which needs to be considered when evaluating the injection element design. The briefly presented results obtained with the injector Imp show that it is possible to strongly reduce the large-scale heterogeneities by improving the injector design, thus leading to better mixing efficiency in front of the RD and to an increase in combustion efficiency by the RD.

The simulation of the injector operation under conditions of RD propagation is essential for a proper evaluation of the injector design. However, such a simulation is quite expensive for an optimization process requiring a relatively large number of calculations. One of the further steps to enhance the design methodology could be the accurate modeling of the transitory refill process with a single injection element under conditions of expanding burnt gases produced by the RD. This technique already demonstrated by the authors[19] would give us the possibility to optimize the injector design at affordable cost.

7. Acknowledgement

This study was funded by ONERA.

References

[1] Voitsekhovskii, B. V. Stationary Spin Detonation. *Soviet Journal of Applied Mechanics and Technical Physics*, 3:157-164, May-June 1960

[2] Nicholls, J. A., Cullen, R. E. The feasability of a rotating detonation wave rocket motor. *Technical Report RPL-DTR-64-113*, University of Michigan, 1964

[3] Bykovskii, F. A., Zhdan, S.A. and Verdernikov, E.F. Continuous Spin Detonations. *Journal of Propulsion and Power*, 22(6):1204-1216, 2006.

[4] Zeldovich, Y. To the question of energy use of detonation combustion. *Journal of propulsion and power*, 22(3):588-592, 2006.

[5] Wintenberger, E. and Shepherd, J.E. Thermodynamic cycle analysis for propagating detonations. *Journal of propulsion and power*, 22(3):694-698, 2006.

[6] Davidenko, D. M. and Eude, Y. and Gökalp, I. and Falempin, F. Theoretical and Numerical Studies on Continuous Detonation Wave Engines. *17th AIAA International Space Planes and Hypersonic Systems and Technologies Conference, (AIAA-2011-2334)*

[7] Zhdan, S.A., Mardashev, A.M. and Mitrofanov, V.V. Calculation of the flow of spin detonation in an annular chamber. *Combustion, Explosion, and Shock Waves*, 26(2):210-214, 1990.

[8] Eude, Y., Davidenko, D.M., Gokalp, I. and Falempin, F. Use of the adaptive mesh refinement for 3D simulations of a CDWRE (continuous detonation wave rocket engine). In *17th AIAA International Space Planes and Hypersonic Systems and Technologies Conference*, April 2011.

DOI: 10.13009/EUCASS2017-171

[9] Liu, M. and Zhou, R. and Wang, J.-P. Numerical Investigation of Different Injection Patterns in Rotating Detonation Engines. *Combustion, Science and Technology*, 187:343-361, 2015.

[10] Schwer, Douglas and Kailasanath, Kailas. Feedback into Mixture Plenums in Rotating Detonation Engines. *50th AIAA Aerospace Sciences Meeting including the New Horizons Forum and Aerospace Exposition, (AIAA-2012-0617).*

[11] Refloch, A. et al. CEDRE software. *AerospaceLab Journal*, Issue 2, 2011, http://www.aerospacelab-journal.org/CEDRE-Software.

[12] Scherrer, D. et al. Recent CEDRE Applications. *AerospaceLab Journal*, Issue 2, 2011, http://www.aerospacelab-journal.org/node/101.

[13] Gaillard, T., Davidenko, D. and Dupoirieux F. Numerical optimisation in non reacting conditions of the injector geometry for a continuous detonation wave rocket engine. *Acta Astronautica*, 111:334-344, 2015.

[14] Davidenko, Dmitry M and Gökalp, Iskender and Kudryavtsev, Alexey N. Numerical simulation of a continuous detonation in a layer of hydrogen-oxygen mixture with periodic conditions, *G.D. Roy and S.M. Frolov (Eds.)*, Deflagrative and detonative combustion (pp.407-422). Moscow: Torus Press (2010), ISBN 978-5-94588-071-9.

[15] Bellenoue, M and Boust, B and Vidal, P and Zitoun, R and Gaillard, T and Davidenko, D and Leyko, M and Le Naour, B. New Combustion Concepts to Enhance the Thermodynamic Efficiency of Propulsion Engines. *AerospaceLab Journal*, 11, 2016.

[16] Stoddard, W.A. and Gutmark, E.J. Comparative Numerical Study of RDE Injection Designs. In *52nd AIAA Aerospace Sciences Meeting*, January 2014.

[17] Stoddard, W.A., George, A.St., Driscoll, R. and Gutmark, E.J. Computational Analysis of Existing and Altered Rotating Detonation Engine Inlet Designs. In *50th AIAA/ASME/SAE/ASEE Joint Propulsion Conference*, July 2014.

[18] Driscoll, R., Aghasi, P., St George, A. and Gutmark, E.J. Three-dimensional, numerical investigation of reactant injection variation in a H_2/air rotating detonation engine. *International Journal of Hydrogen Energy*, 49(9):5162-5175

[19] Gaillard, T., Davidenko, D. and Dupoirieux F. Numerical Investigation of an Unsteady Injection Adapted to the Continuous Detonation Wave Rocket Engine Operation. In *6th EUCASS Conference*, July 2015.